IEEE Access
Multidisciplinary | Rapid Review | Open Access Journal

Received 2 March 2023, accepted 1 April 2023, date of publication 11 April 2023, date of current version 19 April 2023.

Digital Object Identifier 10.1109/ACCESS.2023.3266334

RESEARCH ARTICLE

Research on Electrical Contact Characteristics of Brush-Rail Device With Transient Large Current

YANHAO WU[1], JIN XU[1], JUNJIE ZHU[1], AND WEI XU[2], (Senior Member, IEEE)
[1]National Key Laboratory of Science and Technology on Vessel Integrated Power System, Naval University of Engineering, Wuhan 430033, China
[2]State Key Laboratory of Advanced Electromagnetic Engineering and Technology, Huazhong University of Science and Technology, Wuhan 430074, China

Corresponding author: Jin Xu (xu_1983@yeah.net)

This work was supported in part by the National Natural Science Foundation of China under Grant 51977218.

ABSTRACT An excellent electrical contact state is necessary to ensure safe and stable operation of the system. Therein, contact resistance and arc ablation are essential indexes for estimating the contact state. In view of the characteristics of brush-rail device with transient large current for AC electromagnetic propulsion, a contact resistance model and the concept of arc ablative trigger boundary are proposed in this paper. Firstly, an equivalent circuit model is developed based on structural properties of brush-rail device. Then, the corresponding contact resistance model is established considering the contact pressure, amplitude and frequency of current, sliding velocity and consecutive run times. In addition, the main affecting factors of arc ablation are analyzed and the p-v parameters of arc ablation boundary are determined. Finally, the contact resistance and arc ablative trigger boundary of the brush-rail device are tested on a rotating transient large current experimental platform, which proves the correctness of the proposed method.

INDEX TERMS Electromagnetic propulsion, brush-rail device, equivalent circuit model, contact resistance, arc ablation.

I. INTRODUCTION

An electrical contact refers to the contact between different conductors to carry the current flow [1], which can be divided into fixed contact, separable contact and sliding contact [2], [3]. Among them, the sliding contact is widely used in industry, rail transit, electromagnetic propulsion, such as the commutator in the motor, the arch arc structure in the rail transit [4], the boot rail structure in the subway [5], and the brush-rail device in the electromagnetic propulsion [6], [7]. At present, the electrical devices mainly use AC, and the excellent electrical contact state is a necessary condition to ensure the safe and stable operation of the system. The contact resistance and the arc ablation are essential criteria for measuring the contact state.

In terms of contact resistance model, scholars have worked on mathematical models and experimental method. J. A. Greenwood extracted the formula for estimating shrinkage resistance by using a series of dots representing the connection points between two metal planes [8]. Nakamura assumed a number of cubic points connecting two 3D electrodes, and the shrinkage resistance is calculated by using the finite element method and the boundary element method [9]. The experimental method obtains the current and voltage from the transformer, and then calculates the contact resistance according to Ohm's law. D. H. He studied the change of contact resistance with time and proposed the view that the contact resistance value is not constant in a certain time range, but tends to fluctuate around a median value [10]. Bucca studied the electrical contact between carbon sliders and copper wires and found that the contact resistance is an exponential function of the contact pressure [11]. The existing studies have mainly focused on the contact resistance of the arch arc structure in rail transit, where the state is long time and low current compared to the operating conditions of electromagnetic propulsion.

In terms of arc ablation, most of the existing researches focus on the generation and influence mechanism of arc ablation. Under the influence of the energy produced by the arc, the material of the contact surface sputters out in the form of gas and tiny droplets, leading to arc ablation [12]. At low arc energies, the wear mechanism is dominated by abrasive

The associate editor coordinating the review of this manuscript and approving it for publication was Wenxin Liu.

and adhesive wear. With the increase of arc energy, the wear rate increases sharply, and the wear mechanism is mainly arc ablation [13].

The brush-rail device provides a new idea for electromagnetic propulsion, which can replace the cable power supply to the electrical equipment and thus achieve higher velocity [14]. However, the electrical contact issues may affect the stability and reliability of the device. Different from the traditional structure, the brush-rail device for electromagnetic propulsion are characterized by transient large current [15], so conventional analysis methods are not applicable. Further, this paper will consider transient large current feature of electromagnetic propulsion, including contact resistance and arc ablation, for a specific research of electrical contact characteristics.

Based on what mentioned above, a contact resistance model for the brush-rail device is proposed for transient large current conditions. Therein, the contact resistance model and the concept of arc ablative trigger boundary are proposed. It provides support for the design and safe operation of the brush-rail device. In Section II, the equivalent circuit model of the brush-rail device is built with some assumptions. In Section III, the contact resistance model of the brush-rail device is established according to the influence mechanism of different factors. In Section IV, single variable experiments were performed on a rotating transient large current experimental platform to obtain the corresponding fitting coefficients and to verify the correctness of the model. Meanwhile, the influence mechanism and trigger boundary of arc ablation are analyzed. Conclusions and prospects are drawn in Section V.

II. EQUIVALENT CIRCUIT MODEL

The brush-rail device is shown in Figure 1, R_b, L_b are the resistor, inductor of brush, and R_r and L_r are the resistor, inductor of rail, and $R_1, R_{2,\ldots,}R_n$ are the contact resistors, and $C_{1,\ldots,}C_n$ are the contact capacitors, and n depends on the state of the contact surface.

The power supply is supplied to the electrical equipment through the rail, brush and contact surface. A constant pressure spring applies constant pressure to the brush to keep it attached to the rail. From the micro point of view, the processing cannot achieve absolute smooth, there are many bumps on the contact surface of the brush-rail, and the contact is actually achieved through these bumps. The points formed by these bumps are called conductive spots, which are scattered under contact pressure and current [16].

Electrical contact types can be classified into metallic, quasi-metallic and capacitive contacts based on material properties and contact states. In this way, the electrical contact of the contact surface can be equivalent to the parallel connection of resistors and capacitors, with resistors of various types, including resistors of shrinkage and thin-film type [17]. Thus, the equivalent circuit model for Figure 1 is shown in Figure 2.

In Figure 2, the current flow through the conductive spots. The current around the conductive spot will contract linearly,

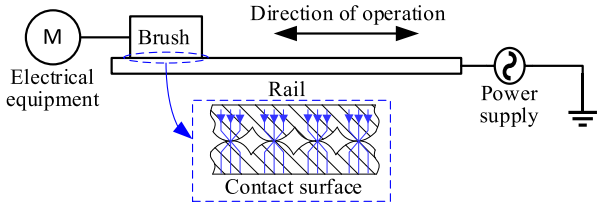

FIGURE 1. Brush-rail device.

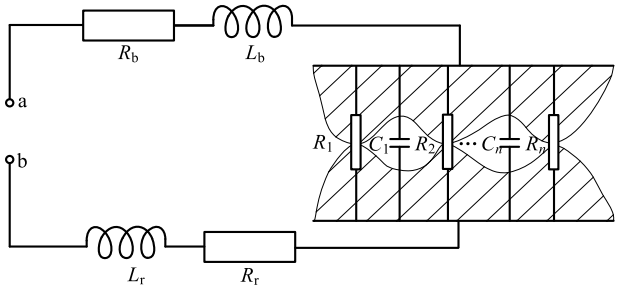

FIGURE 2. Equivalent circuit model.

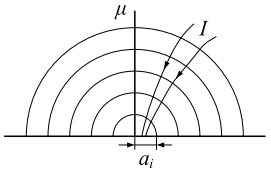

FIGURE 3. Current contraction line.

resulting in a decrease in the effective conductive area, which in turn leads to an increase in the resistance, called the shrinkage resistance R_{ei}.

Assuming that the conductive spot is circular, the equipotential plane around it and the current contraction line as shown in Figure 3. a_i is the radius of the i-th conductive spot, and the Laplace equation of the potential distribution around the conductive spot is:

$$\nabla^2 U(y, r) = 0 \tag{1}$$

The equipotential plane of the ellipsoid is:

$$\frac{r^2}{a_i^2 + \mu^2} + \frac{y^2}{\mu^2} = 1 \tag{2}$$

where, r and y are ellipsoidal coordinates, and μ is an isoplanar parameter of the ellipsoid.

The shrinkage resistance between the equipotential plane and the conductive spot is:

$$R_\mu = \frac{\rho}{2\pi} \int \frac{d\mu}{a_i^2 + \mu^2} = \frac{\rho}{2\pi a_i} \arctan \frac{\mu}{a_i} \tag{3}$$

where, ρ is the resistivity of the material.

When the reference surface is selected as infinite, that is, μ approaches infinite, the shrinkage resistance in half space can be obtained:

$$R_\mu = \frac{\rho}{4a_i} \tag{4}$$

Further, the contact resistance of a single circular conducting spot is the sum of two half-space shrinkage resistances:

$$R_{ei} = \frac{\rho_1 + \rho_2}{4a_i} \tag{5}$$

where, ρ_1 and ρ_2 are the resistivity of the two materials of the contact surface respectively.

The contaminated film on the contact surface increases the resistance of the conducting spot, and the resulting additional resistance is the thin-film resistance R_{fi}:

$$R_{fi} = \frac{\rho_3}{\pi a_i^2} \tag{6}$$

where, ρ_3 is the resistivity of the thin-film resistance of the contact surface.

A single contact resistor is:

$$R_i = R_{ei} + R_{fi} \tag{7}$$

The contact resistance R_c is:

$$R_c = \left[\sum_{i=1}^{n} \frac{1}{R_i}\right]^{-1} \tag{8}$$

A single contact capacitor is:

$$C_j = \frac{\varepsilon S_j}{d_j} \tag{9}$$

where, ε is the dielectric constant, S_j is the surface area of the capacitive contact microelement, d_j is the distance of the capacitive element plate.

As can be seen from Figure 2, capacitive elements and conductive spots are spaced, so the number is approximately the same. The contact capacitance C_c is:

$$C_c = \sum_{i=1}^{n} C_j \tag{10}$$

The expression of impedance Z_{ab} of the two-port network in Figure 2 is:

$$Z_{ab} = R_{ab} + jX_{ab} = R_b + R_r + \frac{R_c}{1 + [\omega C_c R_c]^2} + j\omega\left(L_b + L_r - \frac{C_c R_c^2}{1 + [\omega C_c R_c]^2}\right) \tag{11}$$

where, ω is the angular frequency of the power supply.

In order to analyze the values of each component in the equivalent circuit model, the assumptions are as follows:

(1) The resistance of the brush and rail depends on temperature, material properties, and shape, neglecting changes in value due to wear.

(2) The contact resistance is considerably greater than contact capacitance because the brush-rail device mostly operates with large contact pressure and minor current frequency. Therefore, this paper studies the characteristics of the contact resistance, ignoring the influence of contact capacitance in (11). The contact resistance is:

$$R_c = R_{ab} - R_b - R_r = R_{ab} - \xi\,(R_{b0} + R_{r0}) \tag{12}$$

where, R_{ab} is the resistance of the two-port network ab in Figure 2, obtained from measurements, and ζ is the correction coefficient of skin effect, which is obtained by experiment, and R_{b0}, R_{r0} are the contact resistances of brush and rail without consideration of skin effect, respectively.

(3) During the operation of the brush rail sliding power supply device, the conductive spots will disappear and new ones will be generated. The value of the contact resistance varies only with the operating conditions.

III. ELECTRICAL CONTACT CHARACTERISTICS

The electric contact characteristics can reflect the comprehensive state of the brush-rail device. The affecting factors of contact resistance mainly include contact pressure, current amplitude, current frequency, sliding velocity, consecutive run times and arc ablation.

A. CONTACT PRESSURE

As a result of the contact pressure, the bumps on the contact surface begin to contact each other and form conductive spots. According to the Hertzian elastic contact theory, as the contact pressure increases, the conductive spots formed by contact will undergo elastic deformation, making their radius larger, which will lead to smaller shrinkage resistance and smaller contact resistance [17]. The morphology of conductive spots under different contact pressures is shown in Figure 4.

In (5), the relation between a_i and the contact pressure F can be derived from the Hertz elastic formula:

$$a_i = \xi \sqrt[3]{\frac{3}{4} F \left(\frac{1-\gamma_1^2}{E_1} + \frac{1-\gamma_2^2}{E_2}\right) + \left(\frac{1}{r_1} + \frac{1}{r_2}\right)^{-1}} \tag{13}$$

where, F is the contact pressure, and γ is the Poisson's ratio of the conductive spot, and E is the elastic modulus of the conductive spot, and r is the radius of conductive spot, and ξ is the undetermined coefficient between 0 and 1.

As the contact pressure continues to increase, the conductive spots on the contact surface change from elastic contact to rigid contact, and the variation trend of contact resistance gradually becomes stable. Further, Poisson's ratio, elastic modulus, resistivity and radius of conductive spot are all constants, so (8) can be simplified as:

$$R_c = \frac{p}{F^q} + D \tag{14}$$

where, p, q, D are undetermined coefficients, which are obtained from experimental results.

B. CURRENT AMPLITUDE

The influence of current amplitude on contact resistance is mainly reflected in two aspects: electromotive force and Joule heat.

When the brush-rail device is energized, the current flow through the brush and rail, forming a current loop and generating a magnetic field around them. The current of the

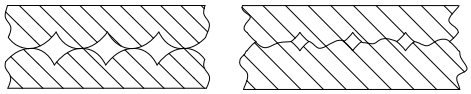

FIGURE 4. Morphology of conductive spots under different contact pressures.

brush and rail will be affected by each other's magnetic field, generating electromotive force, known as Lorentz force.

The electromotive force F_e, is decomposed into F_{ex}, F_{ey} and F_{ez} according to the Cartesian coordinate system. Assuming that the contact pressure is directed along the x-axis, thus F_{ex} can affect the value of the contact pressure in (14), and F_{ex} is proportional to the square of the current, which is:

$$F_{ex} = hI^2 \tag{15}$$

where, I is the value of the current amplitude, and h is the undetermined coefficient, which is determined by the physical structure and can be obtained by finite element analysis. h is positive if in the same direction as the contact pressure, otherwise it is negative.

Current flowing through the contact resistance will generate Joule heat, and its thermal power is:

$$P = (1 - \varepsilon) I^2 R_c \tag{16}$$

where, ε is the material loss rate.

The hardness of metal materials has a negative exponential relationship with temperature, and the hardness will decrease with the increase of temperature. At the same time, with the further increase of temperature, the decrease trend of the material hardness will slow down [18]. The relation between hardness and temperature of metal materials is:

$$H = Ae^{-BT} \tag{17}$$

where, H is material hardness, and T is the temperature, and A is the hardness at absolute temperature of 0, and B is the softening coefficient of material hardness.

As the current amplitude increases, the geometrical morphology and radius of the conductive spot changes, and the larger contact area of the conductive spot decreases the contact resistance. In addition, with the increase of temperature, the resistivity of the material increases, and a larger temperature gradient will increase the heat conduction velocity, both of which will slow down the trend of decreasing contact resistance.

Therefore, the traditional definition of contact resistance as an exponential quadratic function of current amplitude is not accurate. Referring to (16) and (17), the relation between contact resistance and current amplitude considering the influence of Joule heat is:

$$R_c = \left(\frac{p}{(F + F_{ex})^q} + D \right) e^{-\beta I^\alpha} \tag{18}$$

where, α and β are undetermined coefficients, which are related to material properties and obtained by experiment.

C. CURRENT FREQUENCY

The influence of current frequency on contact resistance is reflected in skin effect. The relationship between skin effect depth and current frequency is:

$$\Delta = \sqrt{\frac{\rho}{\pi f \mu_0}} \tag{19}$$

where, f is the current frequency, and μ_0 is the vacuum permeability, and its value is $4\pi \times 10^{-7}$ H/m.

With the increase of current frequency, the skin effect will be more obvious. For brush and rail, the skin effect reduces the effective flow area and increases the contact resistance. Meanwhile, for shrinkage resistance, the penetration depth of electromagnetic field is much greater than a_i, so the effect of current frequency on shrinkage resistance is negligible [19].

When the current frequency is 100 Hz, the penetration depth of skin effect of brush and rail can be calculated by formula (19) as 29.8 mm and 7.3 mm, respectively. Combined with the specific size, it can be seen that the characteristic size of rail is much larger than the penetration depth of magnetic field, so its resistance is more obviously affected by frequency. If the skin effect is not corrected for the resistance of brush and rail, it can be seen from (12) that the calculated value of contact resistance will be greatly affected.

D. SLIDING VELOCITY

On the one hand, with the increase of sliding velocity between the brush and the rail, the gas pressure on the contact surface increases, thus the contact pressure decreases, resulting in the increase of the contact resistance. At the same time, the thickness of the gaseous molecular film also increases, which leads to an increase in the contact gap between the brush and the rail, leading to the increase of the contact resistance.

On the other hand, the friction heat due to mechanical friction will increase the temperature of the contact surface, which is similar to the effect of Joule heat, leading to a decrease in the hardness of the material and thus a decrease in the contact resistance. However, the increase in temperature leads to an increase in the resistivity of the material, which in turn increases the contact resistance.

It can be seen that the factors affecting contact resistance by sliding velocity are complex, and the law between them is traditionally expressed in terms of an exponential function [20], which can be substituted into (18):

$$R_c = \left(\frac{p}{(F + F_{ex})^q} + D \right) e^{kv - \beta I^\alpha} \tag{20}$$

where, v is the sliding velocity of brush and rail; k is the undetermined coefficient, which is related to velocity, material properties, temperature and other factors, and obtained by experiment.

E. CONSECUTIVE RUN TIMES

In transient large current operating conditions, the impact of the contact resistance by the consecutive run times is mainly reflected in the temperature rise. During the operation of the

brush-rail device, the heat source can be divided into Joule heat and friction heat, which both decrease the hardness of the metal material, increase the resistivity, and then change the value of the contact resistance.

As the consecutive run times of the brush-rail sliding power supply structure increases, the temperature of the contact surface increases, but it eventually stabilizes at a certain value. Thus, the relationship between temperature rise and the consecutive run times is:

$$\theta = T_f(1 - e^{-mt}) \tag{21}$$

where, θ is the temperature rise of the contact surface, and t is the consecutive run times, and m is the undetermined coefficient, and T_f is the stable temperature rise of the contact surface. The stable temperature rise corresponds to the balance between the total heat generated by Joule heat and friction and the heat lost through heat dissipation. At this point, the temperature rise does not alter as the increase of the consecutive run times.

Referring to (17), the influence of temperature rise is added to (20), and the contact resistance is:

$$R_c = \left(\frac{p}{(F + F_{ex})^q} + D\right) e^{kv - \beta I^{\alpha} - \tau\theta} \tag{22}$$

where, τ is the undetermined coefficient, which is obtained by experiment.

F. ARC ABLATION

The arc ablation has a serious influence on the brush-rail device, and the extent of the effect is mainly concentrated on the contact surface.

In this way, the ablative brush and rail surfaces form many holes and residues, which increase the roughness of the contact surface. Furthermore, arc ablation induces a chemical reaction on the contact surface of the material, which modifies the resistivity.

However, arc ablation has a strong randomness and uncertainty, so experiments are traditionally used to analyze its affecting factors. Therefore, in the experimental part, this paper studies the affecting factors of arc ablation, including current amplitude, contact pressure and sliding velocity, and explores the trigger boundary of arc ablation.

IV. EXPERIMENT

In order to investigate the influence law and mechanism of the electrical contact characteristics of the brush-rail device, a rotating transient large current experimental platform was developed as shown in Figure 5.

The experimental platform is composed of asynchronous motor, motor controller, brush, rail, constant pressure spring, super capacitor, high power converter and load, etc. Among them, brush, rail materials are metal graphite CT73 and chrome-zirconium copper C18150. The experimental platform can flexibly adjust contact pressure from 0 to 200 N, current amplitude from 0 to 3 kA, current frequency from 1 to 100 Hz, and sliding velocity from 0 to 75 m/s.

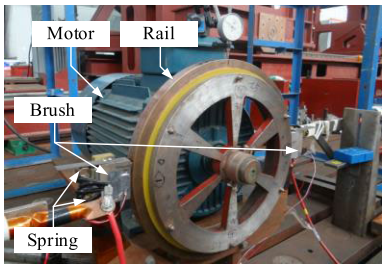

FIGURE 5. Rotating transient large current experimental platform.

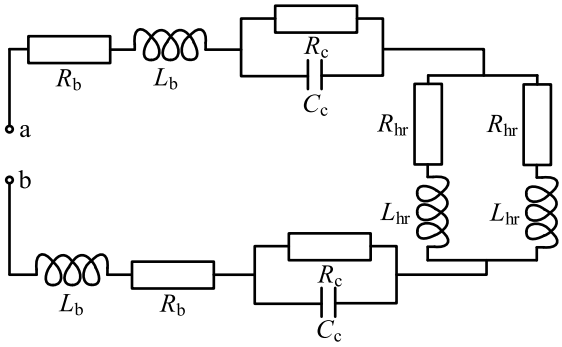

FIGURE 6. Equivalent circuit model of rotating transient large current experimental platform.

Thus, the equivalent circuit model for the rotating transient large current experimental platform is shown in Figure 6. R_{hr} and L_{hr} are the resistance and inductance corresponding to the half circumference of the rail.

The voltage and current signals of the two-port ab in Figure 6 are collected, and then the resistance value corresponding to the fundamental signals of the equivalent circuit model is calculated by voltammetry method.

The simplified contact resistance is:

$$R_c = \frac{1}{2}R_{ab} - R_b - \frac{1}{4}R_{hr} \tag{23}$$

The single variable experiments of contact pressure, current amplitude, current frequency, sliding velocity and consecutive run times were carried out on the experimental platform. At the same time, the affecting factors and trigger boundary of arc ablation are studied.

A. CONTACT PRESSURE EXPERIMENT

The experiment of contact pressure was carried out on the experimental platform. The contact pressure was set to 20 N, 60 N, 100 N, 140 N and 200 N, the current amplitude to 1 kA, the current frequency to 10 Hz, and the sliding velocity to 0 m/s. The temperature was ensured to fluctuate within a limited range during the experiment, and the experiment results of the contact resistance under different contact pressures are shown in Figure 7.

In Figure 7, the contact resistance decreases with the increase of contact pressure. When the contact pressure reaches 100 N, the change trend of contact resistance slows

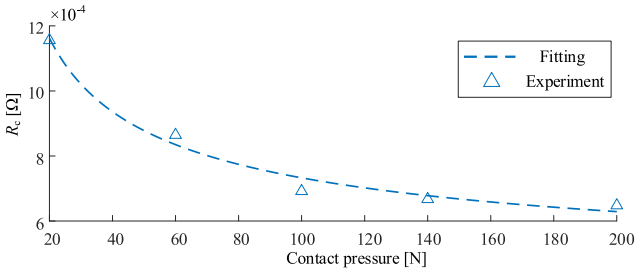

FIGURE 7. Curve of contact resistance and contact pressure.

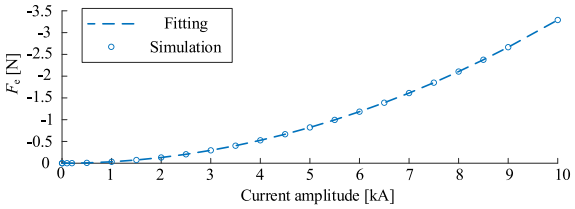

FIGURE 8. Curve of electromotive force and current amplitude.

down. The undetermined coefficient $p = 0.003378$, $q = 0.4833$, $D = 0.000368$, the maximum error of the fitting value is 2.95%, and the average error is 0.83%, indicating that (14) can better fit the experimental value.

B. CURRENT AMPLITUDE EXPERIMENT

The finite element analysis model was built according to the experimental platform to verify the magnitude of the electromotive force. With the contact pressure direction as the positive reference direction, the simulation result of the electromotive force in this direction for different current amplitudes is shown in Fig. 8.

The electromotive force is 0 in the y-axis and z-axis directions and negative in the x-axis directions, indicating that the electromotive force is in the opposite direction to the contact pressure. With the increase of current amplitude, the electromotive force decreases quadratically, which proves that equation (15) is correct and the value of h is -3.29×10^{-2}.

For the Joule heat influence experiments, the contact pressure was set to 20 N, 60 N and 100 N, the current amplitude from 0.2 to 3 kA, the current frequency to 10 Hz, and the sliding velocity to 0 m/s. The temperature was ensured to fluctuate within a limited range during the experiment, and the experiment results of the contact resistance under different current amplitudes are shown in Figure 9.

In Figure 9, the contact resistance decreases with the increase of current amplitude. When the contact pressure was 20 N, 60 N and 100 N, the corresponding undetermined coefficients α are 0.7052, 0.8517 and 0.9157, and β are 0.7231, 0.4514 and 0.3024, respectively. The maximum errors were 28.45%, 14.32% and 4.15% for contact pressures of 20 N, 60 N and 100 N, respectively, with average errors of 8.31%, 4.94% and 1.87%, indicating that the greater the contact pressure, the smaller the error and the less randomness. As the current amplitude increases, the contact resistance decreases and the trend slows down, which additionally explains the correctness of (17) and (18).

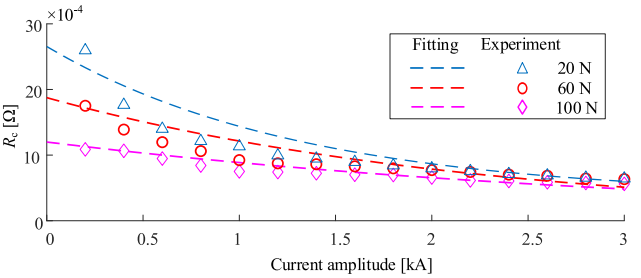

FIGURE 9. Curve of contact resistance and current amplitude.

C. CURRENT FREQUENCY EXPERIMENT

The experiment of current frequency was carried out on the experimental platform. The contact pressure was set to 100 N, the current amplitude from 0.5 to 3 kA, the current frequency from 5 to 100 Hz, and the sliding velocity to 0 m/s. The temperature was ensured to fluctuate within a limited range during the experiment, the experiment results of the resistance of the two-port network R_{ab} are shown in Figure 10.

In Figure 10, as the current frequency increases, the resistance of the two-port network ab increases because of the skin effect that increases the resistance of the brush and rail. Through experimental fitting, the correction coefficient of skin effect is:

$$\eta = 0.04982f + 1 \tag{24}$$

In addition, because the contact resistance is affected by the current amplitude, the resistance of the two-port network ab is different.

D. SLIDING VELOCITY EXPERIMENT

The experiment of sliding velocity was carried out on the experimental platform. The contact pressure was set to 20 N, 60 N and 100 N, the current amplitude to 2 kA, the current frequency to 10 Hz, and the sliding velocity from 0 to 75 m/s. The temperature was ensured to fluctuate within a limited range during the experiment, and the experiment results of the contact resistance under different sliding velocity are shown in Figure 11.

In Figure 11, the contact resistance increases with the increase of sliding velocity. When the contact pressure was 60 N and 100 N, the corresponding undetermined coefficients k are 0.01 and 0.0063. The maximum errors were 15.52% and 4.33% for contact pressures of 60 N and 100 N, respectively, with average errors of 5.71% and 1.12%, indicating that (20) can better fit the experimental value.

In addition, for the contact pressure of 20 N and the sliding velocity of 23 m/s, the contact resistance jumps significantly and increases with the sliding velocity. This is due to the apparent arc ablation at sliding velocities of 23 m/s or above, and the proposed model cannot solve the nonlinear case, which is analyzed in detail later.

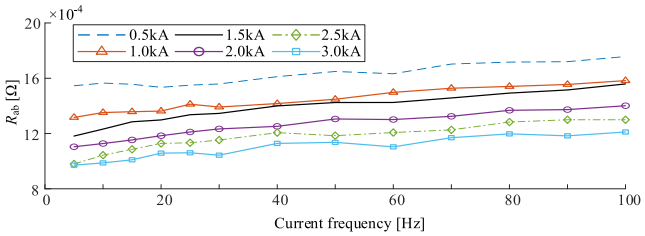

FIGURE 10. Curve of two-port network resistance and current frequency.

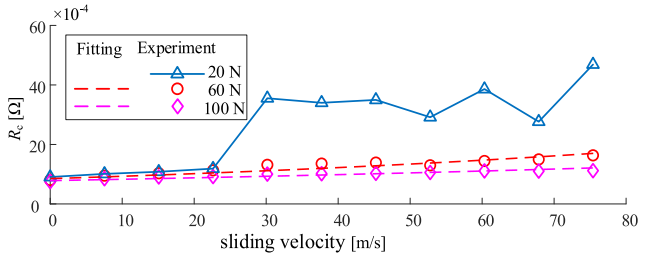

FIGURE 11. Curve of contact resistance and sliding velocity.

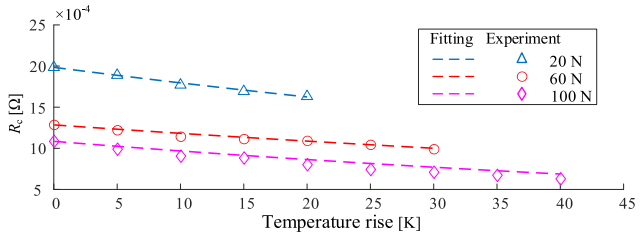

FIGURE 12. Curve of contact resistance and temperature rise.

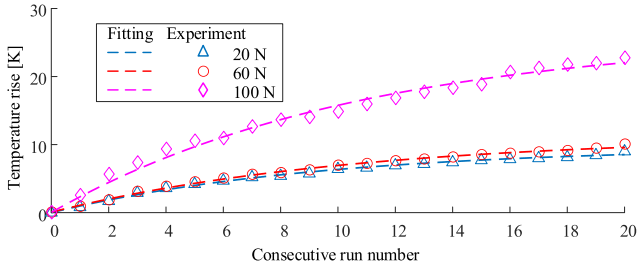

FIGURE 13. Curve of temperature rise and consecutive run times.

E. CONSECUTIVE RUN TIMES EXPERIMENT

The experiment of temperature rise was carried out on the experimental platform. The contact pressure was set to 20 N, 60 N and 100 N, the current amplitude to 0.5 kA, the current frequency to 10 Hz, and the sliding velocity to 0 m/s. The temperature rise of the brush-rail device was increased to a stable value by controlling motor rotation. The contact resistance was measured once for each 5 K decrease in temperature rise, and the experimental results are shown in Figure 12.

In Figure 12, the contact resistance gradually decreases with the increase of temperature rise, which is caused by the decrease of material hardness. When the contact pressure was 20 N, 60 N and 100 N, the corresponding undetermined coefficients τ are 0.01, 0.0083 and 0.0114, the maximum errors are 4.52%, 3.87% and 3.89%, and the average errors are 1.42%, 1.51% and 1.24%, indicating the correctness and applicability of (22).

Further, in order to analyze the relationship between the temperature rise and the consecutive run times, the following operating conditions were set:

1) The rail accelerates from 0 to 45 m/s in 8 s, during which time the two-port network ab through the current flow with an amplitude of 1 kA and a frequency of 10 Hz.

2) The rail decelerates to 0 in 16 s, and rests for 6 s, during which time no current flow.

3) The contact pressure was set to 20 N, 60 N, and 100 N, and the above procedure was repeated 20 times.

Record the average temperature rise during each operation, and the experimental results are shown in Figure 13.

In Figure 13, for contact pressures of 20 N, 60 N and 100 N, the stable temperature rise of the contact surface T_f are 9.69, 11.17 and 26.11, and the corresponding undetermined coefficients m are 0.1067, 0.09525 and 0.09214. The maximum errors were 4.11%, 3.84% and 5.42% for contact pressures of 20 N, 60 N and 100 N, respectively, with average errors of 1.07%, 1.29% and 1.98%, indicating that (21) can better fit the relationship between temperature rise and consecutive run times.

Under the same consecutive run times, the temperature rise is higher when the contact pressure is 100N, because the heat of friction is proportional to the friction force, and the friction force is proportional to the contact pressure. Contact pressures of 20 N and 60 N have little difference in temperature rise. This is because a contact pressure of 20 N has a greater contact resistance, and at the same current amplitude, it has a greater Joule heat.

F. CONTACT RESISTANCE MODEL PREDICTION

The predict model of contact resistance (22) proposed in this paper was verified on the experimental platform. The contact pressure was set to 100 N, the current amplitude to 1 kA, the current frequency to 20 Hz, the sliding velocity to 38 m/s, and the consecutive run times to 10. The comparison between predict and experimental values of contact resistance is shown in Figure 14.

As can be seen from Figure 14, the predict values and the experimental value are mainly consistent in trend, with the maximum error of 6.91% and the average error of 1.5%. It shows that the contact resistance model proposed in this paper could accurately reflect the actual situation of brush-rail device, and has some promising engineering applications.

G. ARC ABLATION EXPERIMENT

In order to investigate the influence of arc ablation on the contact surface of carbon brush, optical electron microscope and white light interferometer are used to photograph and scan the contact surface to compare the contact surface images and roughness before and after arc ablation, as shown in Figure 15 and Figure 16.

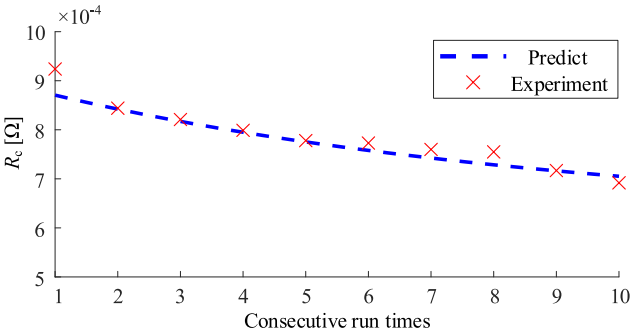

FIGURE 14. Comparison of predict and experimental values of contact resistance.

FIGURE 15. Comparison of brush contact surface images before and after arc ablation.

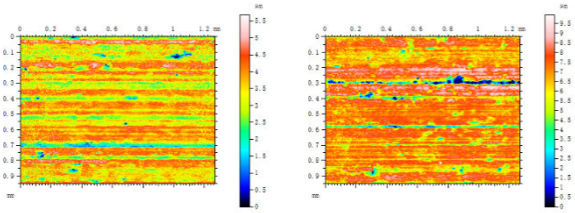

FIGURE 16. Comparison of brush contact surface roughness before and after arc ablation.

For calculating the contact resistance before and after the arc ablation, the contact pressure was set to 100 N, the current amplitude to 2 kA, and the current frequency to20 Hz. The contact resistance before and after arc ablation is 0.6198 mΩ and 0.6483 mΩ respectively, and the roughness before and after arc ablation is 0.562 Sa and 1.83 Sa respectively. It can be known from Figure 15 and 16 that:

1) Arc ablation results in rough contact surfaces, which are exacerbated as the arc ablation, resulting in a decrease in resistive contact, which in turn increases the contact resistance.

2) As the brush and rail slide, the arc ablation residue attached to the brush and rail will further increase the roughness of the contact surface, causing damage to brush-rail device.

In order to objectively evaluate the severity of arc ablation, the voltage waveform of the two-port network ab is used as judgment criterion. It is considered that a single voltage peak represents the occurrence of a single arc ablation. Three evaluation levels are defined as light, medium and heavy,

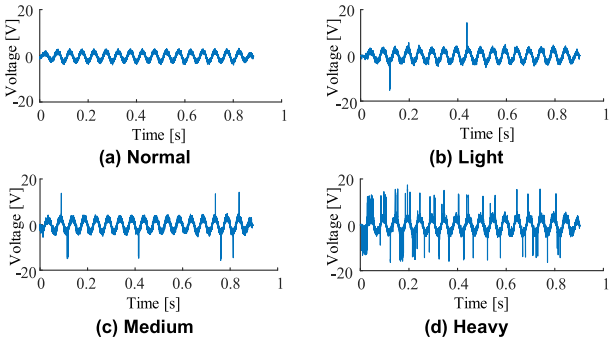

FIGURE 17. Evaluation levels of arc ablation.

corresponding to the occurrence of 1∼2, 3∼7 and more than 8 arc ablations per unit time. The corresponding voltage waveforms for the normal and the three evaluation levels are shown in Figure 17.

The current amplitude, contact pressure, and sliding velocity are investigated for the influence factor of arc ablation in rail transit [21]. Current is a necessary condition for arc ablation [22]. In order to verify the effect of the current amplitude on the arc ablation, the contact pressure was set to 20 N, the current amplitude from 0.5 to 3 kA, the current frequency to 20 Hz, and the sliding velocity to 75 m/s. During the experiments, the arc ablation phenomenon was observed by combining the high-speed camera and voltage waveform. The experiment results of the arc ablation under different current amplitude are shown in Figure 18. The arc ablation phenomenon at current amplitudes of 0.5 kA and 1kA is not obvious, so the degree of arc ablation is judged by the voltage waveform.

In Figure 18, arc ablation occurs at different current amplitudes for certain contact pressures and sliding velocities. The arc ablation becomes more severe with the increase of current amplitude, indicating a positive correlation between the arc ablation and current amplitude.

The experiment of dynamic sliding electrical contact shows that the contact pressure and the sliding velocity are the main causes of arc ablation. The arc ablative trigger boundary value of contact pressure and sliding velocity (p-v) are verified on the experimental platform. The contact pressure was set from 20 to 80 N, the current amplitude to 2 kA, the current frequency to 20 Hz, and the sliding velocity from 0 to 75 m/s. The evaluation level of the arc ablation is judged by the voltage waveform, and the experimental results are shown in Figure 19, where the dots represent individual experiments.

For the same contact pressure from 20 N to 40 N, the arc ablation becomes more severe as the sliding velocity increases, indicating that the arc ablation is positively correlated with the sliding velocity. In the contact pressure range of 20 N to 40 N, arc ablation becomes more severe with the decrease of contact pressure at the same sliding velocity, indicating that arc ablation is negatively correlated with contact pressure. Therefore, in order to avoid the arc ablation of

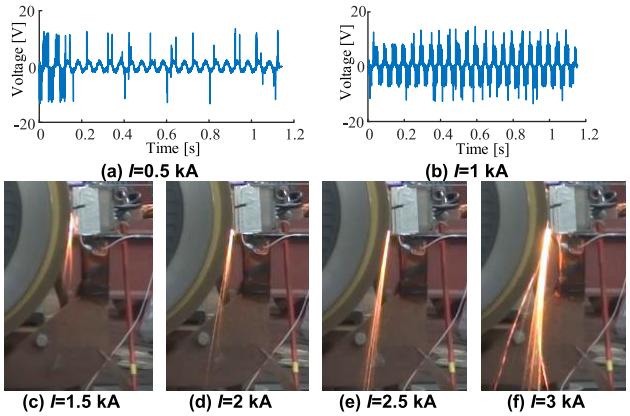

FIGURE 18. Variation of arc ablation with current amplitude.

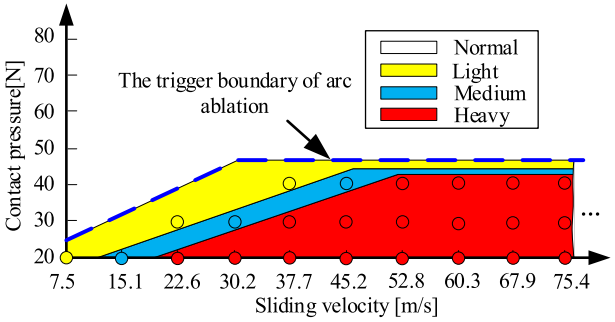

FIGURE 19. Arc ablations trigger boundaries with respect to contact pressure and sliding velocity.

brush-rail device at any sliding velocity, the contact pressure should not be less than 40 N.

In addition, the trigger boundary of arc ablation is related to the geometry and environment of the brush rail device. In order to avoid arc ablation of the brush rail device, a certain safety margin should be increased based on the trigger boundary. The greater the contact resistance, the worse the contact state, and the easier it is to approach or reach the trigger boundary. Combined with the contact resistance model solved earlier in this paper, arc ablation can be further avoided.

V. CONCLUSION

The brush-rail device with transient large current for AC electromagnetic propulsion is taken as the research object in this paper. According to the structure characteristics of the brush-rail device, its equivalent circuit model was established and the rotating transient large current experimental platform was designed. The contact resistance prediction model of the brush-rail device is proposed based on the analysis of different influencing factors, and verified on the experimental platform. The results show that the proposed model can accurately predict the contact resistance under different operating conditions.

The evaluation level of arc ablation is defined, which can objectively describe the severity of arc ablation in the paper. The arc experiment is carried out and the results indicate that arc ablation can change the material properties and increase the roughness of the contact surface, thus increasing the contact resistance; the current amplitude affects the severity of arc ablation, but it is not the main factor affecting the occurrence of arc ablation; the main factors affecting the occurrence of arc ablation are the contact pressure and sliding velocity, and their boundary value for avoiding the arc ablation is determined.

The research results in the paper can provide effective guidance for the parameter design of brush-rail device, and support the precise modeling and control of electromagnetic propulsion equipment. For future studies, the effect of arc ablation on service life will be analyzed based on the research presented here.

REFERENCES

[1] W. Ren, Y. Chen, Z. Wang, S. Xue, and X. Zhang, "Electrical contact resistance of coated spherical contacts," *IEEE Trans. Electron Devices*, vol. 63, no. 11, pp. 4371–4379, Oct. 2016.

[2] D. Gonzalez, M. Hopfeld, F. Berger, and P. Schaaf, "Investigation on contact resistance behavior of switching contacts using a newly developed model switch," *IEEE Trans. Compon., Packag., Manuf. Technol.*, vol. 8, no. 6, pp. 939–949, Jun. 2018.

[3] W. He, Y. Feng, S. Wu, and W. Wang, "Effect of elastoplastic thermal softening on electrical contact resistance based on the dual-iterative coupling method," *IEEE Trans. Dielectr. Electr. Insul.*, vol. 30, no. 1, pp. 11–19, Feb. 2023.

[4] Y. A. Wang, J. X. Li, Y. Yan, and L. J. Qiao, "Effect of pv factor on sliding friction and wear of copper-impregnated metallized carbon," *Wear*, vol. 289, pp. 119–123, Jun. 2012.

[5] L. Yan, "Development and application of the Maglev transportation system," *IEEE Trans. Appl. Supercond.*, vol. 18, no. 2, pp. 92–99, Jun. 2008.

[6] K. Dai, Y. Yang, Q. Yin, and H. Zhang, "Theoretical model and analysis on the locally concentrated current and heat during electromagnetic propulsion," *IEEE Access*, vol. 7, pp. 164856–164866, 2019.

[7] D. Zhou, M.-X. Wei, J. Cao, L. Shi, J. Shen, and L. An, "Simulation and experimental study of the field distribution of engine for electromagnetic pulse," *IEEE Access*, vol. 10, pp. 118475–118483, 2022.

[8] J. A. Greenwood, "Constriction resistance and the real area of contact," *Brit. J. Appl. Phys.*, vol. 17, no. 12, pp. 1621–1632, Dec. 1966.

[9] M. Nakamura and I. Minowa, "Film resistance and constriction effect of current in a contact interface," *IEEE Trans. Compon., Hybrids, Manuf. Technol.*, vol. 12, no. 1, pp. 109–113, Mar. 1989.

[10] D. H. He and R. Manory, "A novel electrical contact material with improved self-lubrication for railway current collectors," *Wear*, vol. 249, no. 7, pp. 626–636, Jul. 2001.

[11] G. Bucca, A. Collina, R. Manigrasso, F. Mapelli, and D. Tarsitano, "Analysis of electrical interferences related to the current collection quality in pantograph–catenary interaction," *Proc. Inst. Mech. Eng., F, J. Rail Rapid Transit*, vol. 225, no. 5, pp. 483–500, Sep. 2011.

[12] Z. Yin, P. Sun, W. Sima, L. Li, W. Du, and H. Sui, "Thermal response properties and surface insulation failure mechanism of epoxy resin under arc ablation," *IEEE Trans. Dielectr. Electr. Insul.*, vol. 26, no. 5, pp. 1503–1511, Oct. 2019.

[13] S. Kubo and K. Kato, "Effect of arc discharge on the wear rate and wear mode transition of a copper-impregnated metallized carbon contact strip sliding against a copper disk," *Tribol. Int.*, vol. 32, no. 7, pp. 367–378, Jul. 1999.

[14] S. Liu, B. Wang, and L. Zhang, "A method for blind source separation of multichannel electromagnetic radiation in the field," *IEEE Access*, vol. 8, pp. 191341–191354, 2020.

[15] H. Zhang, K. Dai, and Q. Yin, "Ammunition reliability against the harsh environments during the launch of an electromagnetic gun: A review," *IEEE Access*, vol. 7, pp. 45322–45339, 2019.

[16] W. Ren, C. Zhang, and X. Sun, "Electrical contact resistance of contact bodies with cambered surface," *IEEE Access*, vol. 8, pp. 93857–93867, 2020.

[17] R. Holm, *Electric Contacts Hand Book*. Cham, Switzerland: Springer-Verlag, 1958.
[18] Y. Kim and H. Y. Choi, "A geometric design study of high-temperature position sensors," *IEEE Sensors J.*, vol. 16, no. 19, pp. 7065–7072, Oct. 2016.
[19] J. D. Lavers and R. S. Timsit, "Constriction resistance at high signal frequencies," *IEEE Trans. Compon. Packag. technol.*, vol. 25, no. 3, pp. 446–452, Sep. 2002.
[20] A. Rosenkranz, L. Reinert, C. Gachot, and F. Mücklich, "Alignment and wear debris effects between laser-patterned steel surfaces under dry sliding conditions," *Wear*, vol. 318, nos. 1–2, pp. 49–61, Oct. 2014.
[21] G. Wu, Y. Zhou, G. Gao, J. Wu, and W. Wei, "Arc erosion characteristics of CU-impregnated carbon materials used for current collection in high-speed railways," *IEEE Trans. Compon., Packag., Manuf. Technol.*, vol. 8, no. 6, pp. 1014–1023, Jun. 2018.
[22] L. M. Shpanin, G. R. Jones, and J. W. Spencer, "Convoluted arc with flux concentrator for current interruption," *IEEE Trans. Plasma Sci.*, vol. 46, no. 1, pp. 175–179, Jan. 2018.

YANHAO WU was born in Henan, China, in 1989. He received the B.S. degree from the Huazhong University of Science and Technology, Wuhan, China, in 2011, and the M.S. degree from the Naval University of Engineering, Wuhan, in 2013, where he is currently pursuing the Ph.D. degree. His research interests include electrical devices and mechanical system dynamics.

JIN XU was born in Anhui, China, in 1983. He received the M.S. and Ph.D. degrees in electrical engineering from the Naval University of Engineering, Wuhan, China, in 2008 and 2012, respectively. He is currently a Professor and a Supervisor of Ph.D. students. His current research interests include energy storage, electrical devices, linear electric machine design, and its control.

JUNJIE ZHU was born in Jiangsu, China, in 1984. He received the Ph.D. degree in electrical engineering from the Naval University of Engineering, Wuhan, China, in 2013. He is currently a Researcher and a Doctoral Supervisor. His current research interests include power electronics, microgrids, and power quality compensation.

WEI XU (Senior Member, IEEE) was born in Chongqing, China, in 1980. He received the double B.E. and M.E. degrees in electrical engineering from Tianjin University, Tianjin, China, in 2002 and 2005, respectively, and the Ph.D. degree in electrical engineering from the Institute of Electrical Engineering, Chinese Academy of Sciences, in 2008.

From 2008 to 2012, he was a Postdoctoral Fellow with the University of Technology Sydney, a Vice Chancellor Research Fellow with the Royal Melbourne Institute of Technology, and a Japan Science Promotion Society Invitation Fellow with Meiji University. Since 2013, he has been a Full Professor with the State Key Laboratory of Advanced Electromagnetic Engineering, Huazhong University of Science and Technology, China. His research interests include the design and control of linear/rotary machines and drives. He is a fellow of the Institute of Engineering and Technology (IET). He is the General Chair of the 2021 International Symposium on Linear Drives for Industry Applications (LDIA 2021), Wuhan, China, and the 2023 IEEE International Conference on Predictive Control of Electrical Drives and Power Electronics (PRECEDE 2023), Wuhan. He has been an Associate Editor for over ten international peer-reviewed journals, including IEEE TRANSACTIONS ON INDUSTRIAL ELECTRONICS, IEEE TRANSACTIONS ON VEHICULAR TECHNOLOGY, IEEE TRANSACTIONS ON TRANSPORTATION ELECTRIFICATION, IEEE TRANSACTIONS ON ENERGY CONVERSION, and IEEE TRANSACTIONS ON INDUSTRY APPLICATIONS.